The Abdus Salam
International Centre for Theoretical Physics

United Nations
Educational, Scientific and
Cultural Organization

IAEA
International Atomic Energy Agency

2163-29

College on Soil Physics: Soil Physical Properties and Processes under Climate Change

30 August - 10 September, 2010

Wind effects on sediment transport by raindrop-impacted shallow flow: a wind-tunnel study

Gunay Erpul
University of Ankara
Turkey

Earth Surface Processes and Landforms
Earth Surf. Process. Landforms **29**, 955–967 (2004)
Published online in Wiley InterScience (www.interscience.wiley.com). DOI: 10.1002/esp.1077

WIND EFFECTS ON SEDIMENT TRANSPORT BY RAINDROP-IMPACTED SHALLOW FLOW: A WIND-TUNNEL STUDY

G. ERPUL,[1]* D. GABRIELS[2] AND L. D. NORTON[3]

[1] *Faculty of Agriculture, Department of Soil Science, University of Ankara, 06110 Diskapi–Ankara, Turkey*
[2] *Department of Soil Management and Soil Care, Ghent University, Coupure Links 653, B 9000 Ghent, Belgium*
[3] *USDA–ARS National Soil Erosion Research Laboratory, 1196 SOIL Bldg, Purdue University, West Lafayette, IN 47907–1196, USA*

Received 24 January 2003; Revised 16 September 2003; Accepted 16 December 2003

ABSTRACT

In wind-driven rains, wind velocity and direction are expected to affect not only energy input of rains but also shallow flow hydraulics by changing roughness induced by raindrop impacts with an angle on flow and the unidirectional splashes in the wind direction. A wind-tunnel study under wind-driven rains was conducted to determine the effects of horizontal wind velocity and direction on sediment transport by the raindrop-impacted shallow flow. Windless rains and the rains driven by horizontal wind velocities of 6 m s^{-1}, 10 m s^{-1}, and 14 m s^{-1} were applied to three agricultural soils packed into a 20 by 55 cm soil pan placed on both windward and leeward slopes of 7 per cent, 15 per cent, and 20 per cent. During each rainfall application, sediment and runoff samples were collected at 5-min intervals at the bottom edge of the soil pan with wide-mouth bottles and were determined gravimetrically. Based on the interrill erosion mechanics, kinetic energy flux (E_{rn}) as a rainfall parameter and product of unit discharge and slope in the form of $q^b S_o^c$ as a flow parameter were used to explain the interactions between impact and flow parameters and sediment transport (q_s). The differential sediment transport rates occurred depending on the variation in raindrop trajectory and rain intensity with the wind velocity and direction. Flux of rain energy computed by combining the effects of wind on the velocity, frequency, and angle of raindrop impact reasonably explained the characteristics of wind-driven rains and acceptably accounted for the differences in sediment delivery rates to the shallow flow transport ($R_2 \geq 0{\cdot}78$). Further analysis of the Pearson correlation coefficients between E_{rn} and qS_o and q_s also showed that wind velocity and direction significantly affected the hydraulics of the shallow flow. E_{rn} had a smaller correlation coefficient with the q_s in windward slopes where not only reverse splashes but also reverse lateral raindrop stress with respect to the shallow flow direction occurred. However, E_{rn} was as much effective as qS_o in the sediment transport in the leeward slopes where advance splashes and advance lateral raindrop stress on the flow occurred. Copyright © 2004 John Wiley & Sons, Ltd.

KEY WORDS: wind-driven rain; raindrop-induced roughness; unidirectional splashes; sediment transport by shallow flow

INTRODUCTION

Wind has long been known as a factor that has important roles in water erosion processes, but very few studies have been made on the effect of wind on raindrops (Disrud, 1970; De Lima, 1989a, 1990; Pedersen and Hasholt, 1995; Helming, 2001; Erpul *et al*., 2002, 2003a,b) and overland flow characteristics (De lima, 1989a; Gerits and De Lima, 1990; De Lima *et al*., 2003) since the experimental conditions are even now limited. Thus, there still remain significant aspects that are not well understood in erosion processes in situations where wind and rain occur at the same time.

Given generally shallow depths of overland flow, detachment by flow is often of minor importance for interrill erosion (Foster, 1982), and therefore interrill detachment is considered to be mainly due to raindrop impact. As a result of rainsplash of soil particles within shallow flow, raindrop-impacted overland flow can transport soil particles in the flow direction even if there is very shallow flow. This process differs from the transport by both overland flow without raindrop impact and rill flow, which must attain a critical velocity to set soil particles in motion. Typically, the basic processes of raindrop-impacted shallow flow are detachment by raindrop impact and

* Correspondence to: G. Erpul, Faculty of Agriculture, Department of Soil Science, University of Ankara, 06110 Diskapi–Ankara, Turkey. E-mail: erpul@agri.ankara.edu.tr

transport by overland flow (Julien and Simons, 1985; Guy *et al*., 1987; Kinnell, 1993; Parsons *et al*., 1998; Zhang *et al*., 1998).

Results of laboratory experiments on the significance of wind on raindrop impact and rainsplash detachment have recently been reported by Erpul *et al*. (2003a). They found differential rates to occur depending on the changes in raindrop fall trajectory and raindrop frequency with the wind velocity and direction. Energy flux of rain computed by combining the effects of wind on the velocity, angle, and frequency of raindrop impact reasonably predicted the mass of sediments detached from the bare soil surface by the impacts of wind-driven raindrops. Although rainsplash transport falls to a large extent with the flow depth range of 0–2 mm, and beyond it becomes negligible (Ghadiri and Payne, 1981; Torri *et al*., 1987), rainsplash detachment can still be active at greater flow depths (Moss and Green, 1983; Kinnell, 1988, 1990).

A splash corona is created when a raindrop impacts shallow flow covering a soil surface, and soil detachment results from these splashes (Mutchler, 1967; Mutchler and Larson, 1971; Mutchler and Young, 1975; Ghadiri and Payne, 1980; Poesen and Savat, 1981). Vertically falling and uniformly distributed raindrop impacts on a uniform soil surface induce symmetric splashes from the corona edge in all directions that result in a null net transport of sediments. However, the impact of a wind-driven raindrop causes an asymmetric splash corona, which is distorted towards the direction of the wind, and in addition to distorting raindrop splash, wind also has an important role in deviating trajectories of splash droplets towards the direction of wind (De Lima, 1989b). Therefore, wind velocity and direction are expected to affect not only rainsplash detachment but also shallow flow hydraulics by changing roughness induced by raindrop impacts on flow with an angle and by their asymmetric and directional splashes, whether submerged or not, in relation to the downward shallow flow.

The growth of wind-induced waves on the flow is also likely to have a role in shallow flow hydraulics. De Lima (1989c) explored the effects of raindrops driven by wind velocities of 4·6 and 5·7 m s^{-1} and wind disturbances on overland flow on an impervious surface, and concluded that the effects of tangential wind shear stress exerted on the flow surface and splashes were smaller than the effect of the lateral stress of impacting wind-driven raindrops for high intensity rainfalls. Nevertheless, they could be significant when a shallow flow depth covers the entire soil surface under low intensity rainfalls.

De Lima *et al*. (2003) have studied how storm velocity and direction influenced water erosion, and the results showed that the soil loss caused by the downstream-moving rainstorms was greater than that caused by identical upstream-moving rainfall storms. In the present study, sediment transport rates by raindrop-impacted shallow flow were measured under wind-driven rain. By comparing the results from windward and leeward slopes, we aimed to clarify the effects of wind velocity and direction on the transport process.

MATERIALS AND METHODS

The study was conducted in a wind tunnel rainfall simulator facility at Ghent University, Belgium (Gabriels *et al*., 1997). The wind tunnel is a closed circuit and low speed type wind tunnel made of sheet metal. An axial fan, which is 1·5 m in diameter and has 16 adjustable blades driven by a 200 hp electric motor, generates airflow. Adjusting the pitch angle of the blades by means of a compressor controls the wind speed, and the minimum free stream wind velocity is 6·0 m s^{-1} in the tunnel. The air current is streamlined as it passes a screen and a 2·60 m long cross-shaped splitter, and fixed air straightener vanes are placed in front of the fan to remove the swirl induced by rotation of the blades. Wind streams additionally pass a honeycomb system before entering into the working area (test section). A particle-settling chamber allows sedimentation of air load and is vented to the atmosphere by means of a breather to protect drifting of static pressure in the tunnel. Wind velocity profiles above wind tunnel floor are characterized by the following logarithmic equation:

$$u(z) = \left(\frac{u_*}{\kappa}\right)\ln\left(\frac{z}{z_o}\right) \text{ for } z > z_o \tag{1}$$

where $u(z)$ is the wind velocity at height z, z_o is the aerodynamic roughness height, u_* is the wind shear velocity, and κ is von Karman's constant. Average wind velocity profiles regardless of slope gradient and aspect with a

fixed roughness height of 0·0001 m for a bare and smoothed soil surface are $0{\cdot}0001e^{1{\cdot}1148u}$, $0{\cdot}0001e^{0{\cdot}7480u}$, and $0{\cdot}0001e^{0{\cdot}5142u}$, and the corresponding reference shear velocities (u_*) are 0·35, 0·53, and 0·77 m s^{-1} for the reference wind velocities of 6, 10, and 14 m s^{-1}, respectively. These are the profiles in the form of:

$$z = ae^{bu} \tag{2}$$

where $a = z_o$ and $b = \kappa/u_*$. It is important here to note that the effect of rain load on the reference wind velocities was unknown during the wind-driven rain simulations due to the fact that anemometers suitable to work under rainy conditions were not available during simulations. The logarithmic profile in the air–water interface introduces a flow resistance, which is related to the wind shear velocity, $u_* = (\tau_w/\rho_a)^{1/2}$, where τ_w is the shear stress exerted on the flow surface by wind, and ρ_a is the air density. Since the wind disturbances on the flow will be much less than the flow resistance induced by the raindrop impacts in wind-driven rains (De Lima, 1989c) and given the size of the soil pan (55 by 20 cm), which has a very limited length to generate waves, we assumed a minor effect of wave-induced perturbations in our experiments.

All experiments are conducted in the working area, which is 1·20 m wide and 12 m long with the ceiling adjustable in height from 1·80 m to 3·20 m. The wind tunnel allows study of the combined effect of wind and rain on soil erosion. This is made possible by the installation of a rainfall simulator at the ceiling of the working area of the wind tunnel over a length of 12 m. The rainfall simulator consists of a pipeline with spray nozzles. In this study, we used a continuous spraying system of ten downward-oriented nozzles installed at 2 m high and 1 m intervals. Nozzle pressure was kept at 1·50 bar. Erpul *et al*. (1998, 2000) give a detailed description of the raindrop size distribution for simulated rainfall in the wind tunnel. The simulated rainfall in the wind tunnel consists of rather small raindrops ranging from 0·2 to 1·8 mm for windless rains and up to 3 mm for wind-driven rains. The nozzles at 1·5 bar operating pressure deliver a median raindrop size (d_{50}) of 1·00, 1·63, 1·53, and 1·55 mm for windless rain and the rains driven by 6, 10, and 14 m s^{-1}, respectively. Values of d_{25}, d_{50}, and d_{75} of wind-driven rainfalls are greater than those of windless rainfalls. This is attributed either to the raindrop collisions expected as a result of a greater number of small raindrops per unit volume of air or to the possibility that small raindrops would drift further away than large drops from the test section of the wind tunnel. There is no significant difference in d_{50} of wind-driven rains, which have smaller 'spreading' (d_{25}/d_{75}) and 'sorting' ($(d_{75} - d_{25})/d_{50}$) coefficients compared to the windless rain. In general, the raindrop sizes of wind-driven rainfalls have a narrow range around d_{50}, and the most dominant raindrop size is 1·8 mm.

The energy of simulated rainfall was measured by a piezoelectric ceramic kinetic energy sensor (Sensit™, model V04, Sensit Co., Portland, ND, USA; Erpul *et al*., 2003a). The kinetic energy sensor is a 5 cm ceramic disc; it works on the piezoelectric effect of a ceramic disc, which produces electric charges proportional to the kinetic energy of impacting raindrops. The Sensit essentially has two outputs: kinetic energy units and number of raindrop impacts. The functional relationship obtained by the kinetic energy sensor between the kinetic energy (KE) and the horizontal wind velocity (u) was in the form of:

$$KE = 6 \times 10^{-6} e^{0{\cdot}2184u} \tag{3}$$

where KE is in joules, and u in m s^{-1}. The calculated resultant impact velocities (v_r) of median drop sizes for the windless rains and the rains driven by the reference wind velocities of 6, 10, and 14 m s^{-1} were $4{\cdot}38 \pm 0{\cdot}58$, $4{\cdot}64 \pm 0{\cdot}56$, $7{\cdot}64 \pm 0{\cdot}60$, and $10{\cdot}48 \pm 0{\cdot}57$ m s^{-1}, respectively. The sensor measurement showed that an exponential relationship existed between the energy of the simulated rains and the horizontal wind velocity. The increase in rain energy was mainly ascribed to the increase in the resultant raindrop impact velocity since the raindrop size distribution did not change significantly, in the rains driven by 6, 10 and 14 m s^{-1} winds in the wind tunnel facility (Erpul *et al*., 1998; 2000, 2003a).

The intensity of simulated rains was directly measured with five small collectors on the inclined plane with respect to the prevailing wind direction. That is, the collectors were placed next to the soil pan with the same slope gradient and aspect as the soil pan during each run. In this way, the intensity measurements were made truly representative for each run without any need for correction due to the rain inclination gained from horizontal wind velocity and slope gradient and aspect (Sharon, 1980; De Lima, 1990). From the direct intensity

measurements, the average angle of rain incidence between the wind vector and the plane of the surface ($\beta \mp \theta$) was calculated using the cosine law of spherical trigonometry (Sellers, 1965):

$$\phi = \frac{I_a}{I} = \cos(\beta \mp \theta) \tag{4}$$

where ϕ is the impact efficiency of wind-driven raindrops, I_a is the actual intensity (mm h^{-1}), I is the rainfall intensity in respect to a plane normal to the rain vector (mm h^{-1}), β is the raindrop inclination from vertical (degree), and θ is the slope gradient (degree). The calculated average rain inclination was $53{\cdot}0 \pm 11{\cdot}5°$, $68{\cdot}2 \pm 7{\cdot}6°$, and $73{\cdot}5 \pm 6{\cdot}6°$ for the rains driven by wind velocities of 6, 10, and 14 m s^{-1}, respectively (Erpul *et al*., 2003a). The angles refer to the average values generalized over the raindrop size range, and the analysis of variance showed that at the level of $\alpha = 0{\cdot}05$ the means were significantly different from each other.

Three loess-derived agricultural soils, Kemmel1 sandy loam (57·6 per cent sand, 31·1 per cent silt, and 11·3 per cent clay) and Kemmel2 loam (37·8 per cent sand, 44·5 per cent silt, and 17·7 per cent clay) from the Kemmelbeek watershed (Heuvelland, West Flanders, Belgium) and Nukerke silt loam (32·1 per cent sand, 52·3 per cent silt, and 15·6 per cent clay) from the Maarkebeek watershed (Flemish Ardennes, East Flanders, Belgium) were used in this study. The soil samples were collected from the A_p horizon and air-dried prior to the experiment. Soil was sieved into three aggregate fractions: 1·00–2·75, 2·75–4·80, and 4·80–8·00 mm, and the weighing factors assigned to each fraction were 28, 32, and 40 per cent, respectively to reconstitute the packing soil. A 5 kg soil sample was then packed loosely into a 55 cm long and 20 cm wide pan after the three fractions of aggregates were evenly mixed.

Windless rains and the rains driven by horizontal wind velocities of 6, 10, and 14 m s^{-1} were applied to the soil pan placed at both windward and leeward slopes of 7, 15, and 20 per cent (Figure 1). For each soil and slope aspect, there were three replicates, or 36 runs for a total of 216 rainfall simulations.

In the present study, we assumed rainsplash detachment rate under inclined rain is related to the normal component of raindrop impact velocity (Heymann, 1967; Springer, 1976; Gilley *et al*., 1985; Gilley and Finkner, 1985; Erpul *et al*., 2003a). Accordingly, the kinetic energy flux (E_{rn}, W m^{-2}) was described by:

$$E_{rn} = \Xi\left(\frac{1}{2}mv_r^2\right)\cos^2(\beta \mp \theta) \tag{5}$$

where m is the mass of the raindrop in kg, and v_r is in m s^{-1}, β and θ are in degrees, and Ξ is the number of raindrops in # m^{-2} s^{-1} and calculated by:

$$\Xi = \frac{I_a}{\forall_{d_{50}}} \tag{6}$$

where I_a is in m s^{-1}, and $\forall_{d_{50}}$ is the volume of median raindrop size in m^3.

Rainfall simulations were conducted under freely drained conditions, and generally steady-state soil loss and runoff rates were attained within 45 min in windless rains and the wind-driven rains on windward slopes. However, particularly in the rains driven by wind velocities of 10 and 14 m s^{-1} on the leeward slopes of 15 and 20 per cent, time to runoff changed greatly, and overland flow generation was retarded due to the lesser amount of rain interception. In these cases, an additional 45 min rainfall run was needed to be able to collect sediment and runoff samples at steady-state rates. During each rainfall application and after runoff started, sediment and runoff samples were collected at 5 min intervals at the bottom edge of the pan using wide-mouth bottles and were determined gravimetrically. Total sediment and runoff values, and the total simulated rainfall duration, were used in calculation of sediment transport rate by rain-impacted shallow flow (q_s). The following log-linear model (SAS, 1995) was analysed for the sediment transport by rain-impacted shallow flow based on interrill erosion mechanics (Julien and Simons, 1985; Gilley *et al*., 1985; Guy *et al*., 1987; Zhang *et al*., 1998; Parsons *et al*., 1998):

$$q_s = kE_{rn}^a q^b S_o^c \tag{7}$$

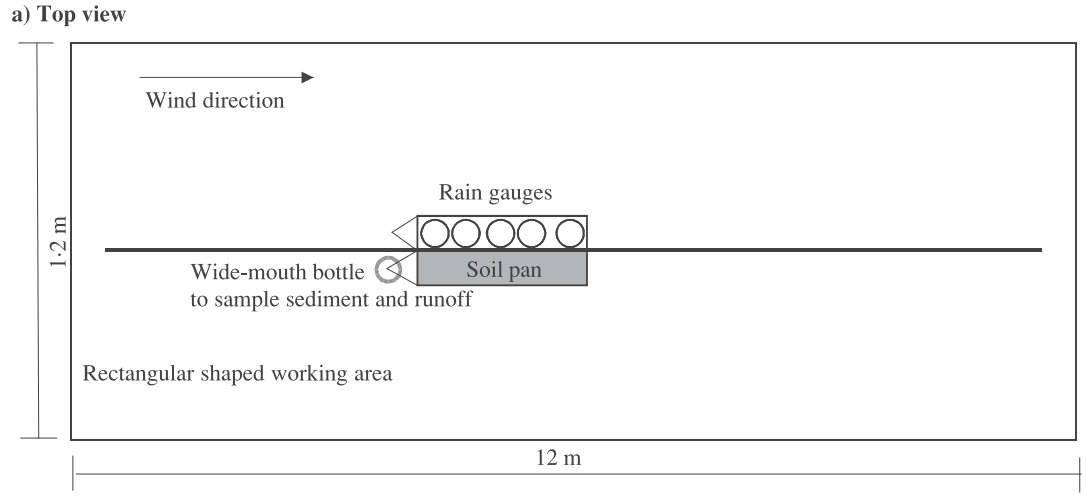

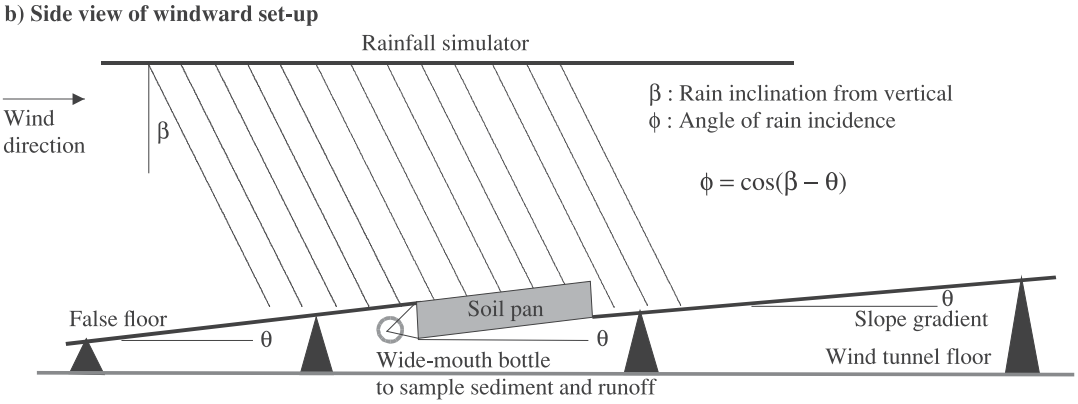

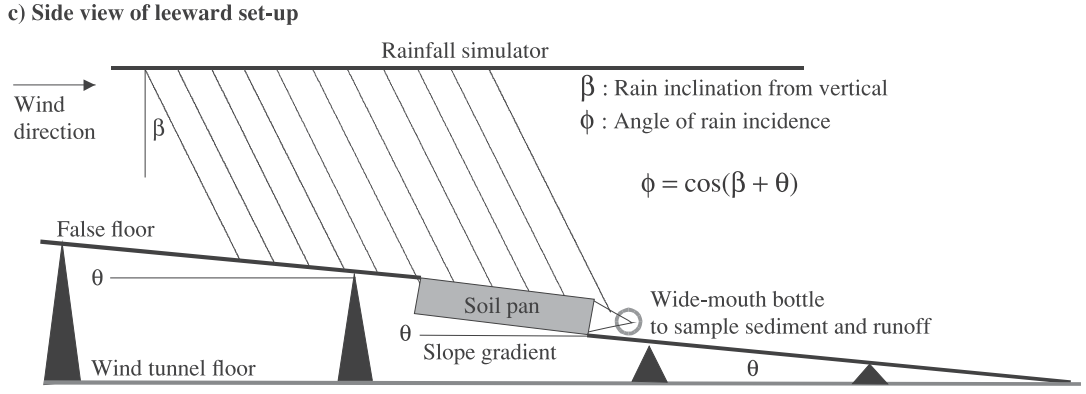

Figure 1. Experimental set-up with soil pan and wide mouth bottle to sample sediment and runoff arranged on the windward and leeward slopes in the wind tunnel

where k is the soil transport parameter for sediment transport by raindrop-impacted shallow flow and, a, b, and c are regression coefficients to which kinetic energy flux, unit discharge and slope are raised, respectively.

RESULTS AND DISCUSSION

Measured rain intensities, angle of rain incidence, and kinetic energy flux for the windless rain and the rains driven by the reference wind velocities of 6, 10, and 14 m s^{-1} are presented in Table I, and a summary of the data used in evaluating sediment transport by rain-impacted shallow flow for three soils is presented in Table II. Differential sediment transport rates occurred depending on the variation in raindrop trajectory and frequency with wind velocity and direction (Figure 2). For a given wind velocity, the transport rate regularly increased on windward slopes due to the greater rain intensities with greater impact angles as the slope gradient increased.

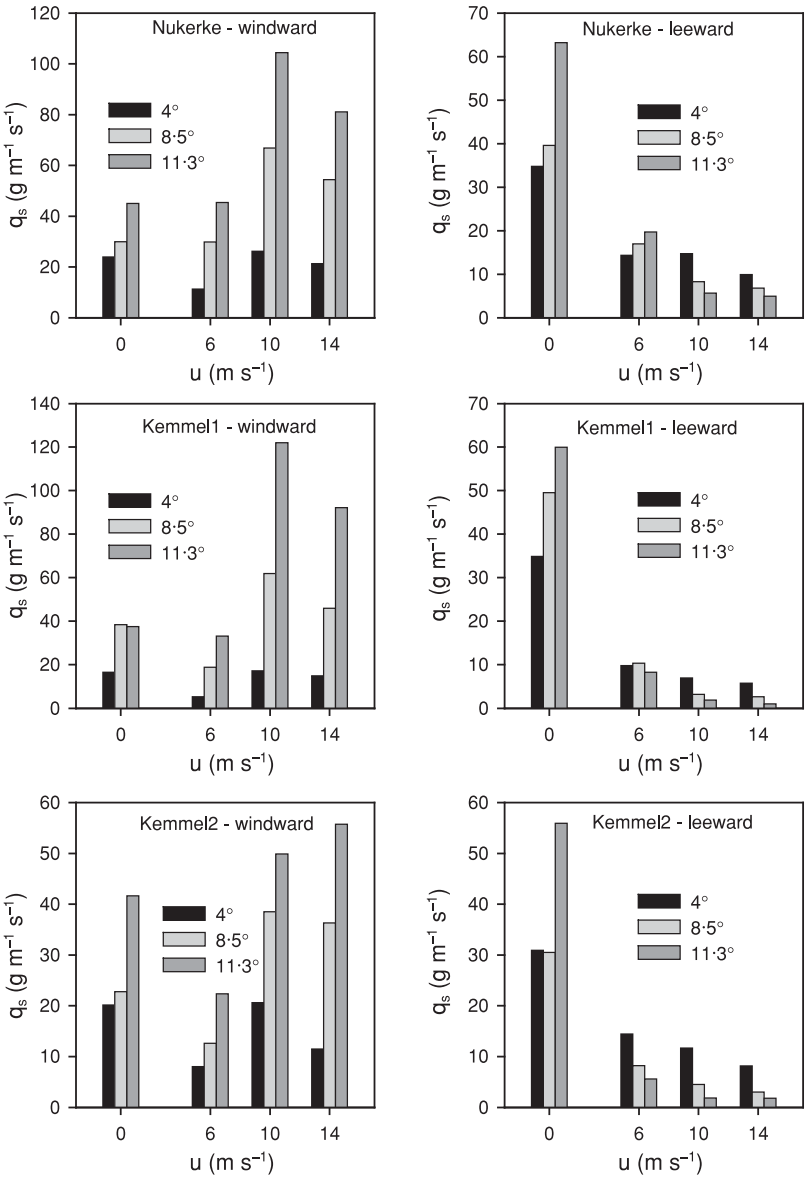

Figure 2. Measured sediment transport rates by raindrop-impacted shallow flow for Nukerke silt loam, Kemmel1 sandy loam, and Kemmel2 loam

Table I. Measured rainfall intensities (I_a), angle of rain incidence ($\beta \pm \theta$), and kinetic energy flux (E_{rn}) for the windless rains and the rains driven by the reference wind velocities of 6, 10, and 14 m s^{-1} (reprinted from Erpul *et al.*, 2003b, with permission from Elsevier)

u (m s^{-1})	v_r (m s^{-1})	d_{50} (mm)	β (°)	S_o (m m^{-1})	θ (°)	I_a (mm h^{-1})	$\beta \pm \theta$ (°)	ϕ	E_{rn} (W m^{-2})
0, ww	4·38 ± 0·58*	1·00	–	0·07	4·0	142	4·0	0·9976	0·377
		0·97 ≤ d_{50} ≤ 1·04†		0·15	8·5	140	8·5	0·9890	0·365
				0·20	11·3	134	11·3	0·9806	0·343
6, ww	4·64 ± 0·56	1·63	53·0 ± 11·5*	0·07	4·0	90	49·0	0·6561	0·116
		1·38 ≤ d_{50} ≤ 1·84		0·15	8·5	100	44·5	0·7133	0·152
				0·20	11·3	106	41·7	0·7466	0·177
10, ww	7·64 ± 0·60	1·53	68·2 ± 7·6	0·07	4·0	120	64·2	0·4352	0·184
		1·50 ≤ d_{50} ≤ 1·57		0·15	8·5	130	59·7	0·5045	0·268
				0·20	11·3	131	56·9	0·5461	0·317
14, ww	10·48 ± 0·57	1·54	73·5 ± 6·6	0·07	4·0	90	69·5	0·3502	0·168
		1·51 ≤ d_{50} ≤ 1·57		0·15	8·5	103	65·0	0·4226	0·281
				0·20	11·3	112	62·2	0·4664	0·372
0, lw	4·38 ± 0·58	1·00	–	0·07	4·0	165	4·0	0·9976	0·438
		0·97 ≤ d_{50} ≤ 1·04		0·15	8·5	172	8·5	0·9890	0·448
				0·20	11·3	179	11·3	0·9806	0·459
6, lw	4·64 ± 0·56	1·63	53·0 ± 11·5	0·07	4·0	126	57·0	0·5446	0·112
		1·38 ≤ d_{50} ≤ 1·84		0·15	8·5	112	61·5	0·4772	0·076
				0·20	11·3	94	64·3	0·4337	0·053
10, lw	7·64 ± 0·60	1·53	68·2 ± 7·6	0·07	4·0	92	72·2	0·3057	0·070
		1·50 ≤ d_{50} ≤ 1·57		0·15	8·5	61	76·4	0·2351	0·020
				0·20	11·3	51	79·5	0·1822	0·014
14, lw	10·48 ± 0·57	1·54	73·5 ± 6·6	0·07	4·0	66	77·5	0·2164	0·047
		1·51 ≤ d_{50} ≤ 1·57		0·15	8·5	42	82·0	0·1392	0·012
				0·20	11·3	34	84·8	0·0906	0·004

u, horizontal wind velocity (ww, windward; lw, leeward); v_r, resultant raindrop impact velocity; d_{50}, median drop size; β, rain inclination from vertical; θ or S_o, slope gradient; ϕ, cosine of angle of rainfall incidence [= cos ($\beta \pm \theta$)].

* Standard deviations of the resultant raindrop impact velocity and the rainfall inclination are given next to the mean value with ± sign.

† 95% confidence interval on mean values of d_{50}.

Table II. Summary of the data for main flow parameters used to evaluate the sediment transport rate by raindrop-impacted shallow flow for three soils* (reprinted from Erpul *et al.*, 2003b, with permission from Elsevier)

u ($m\ s^{-1}$)	S_o ($m\ m^{-1}$)	Nukerke			Kemmel1			Kemmel2			n
		q* ($m^2\ min^{-1}$)	q_s ($g\ m^{-1}\ min^{-1}$)		q ($m^2\ s^{-1}$)	q_s ($g\ m^{-1}\ min^{-1}$)		q ($m^2\ s^{-1}$)	q_s ($g\ m^{-1}\ min^{-1}$)		
			Mean	St dev.		Mean	St dev.		Mean	St dev.	
0	0·07	$3{\cdot}878 \times 10^{-4}$	23·982	2·414	$4{\cdot}935 \times 10^{-4}$	16·566	5·418	$3{\cdot}243 \times 10^{-4}$	20·130	0·839	3
ww	0·15	$4{\cdot}888 \times 10^{-4}$	29·952	3·592	$5{\cdot}100 \times 10^{-4}$	38·394	5·943	$3{\cdot}541 \times 10^{-4}$	22·758	0·963	3
	0·20	$4{\cdot}938 \times 10^{-4}$	45·066	4·005	$5{\cdot}237 \times 10^{-4}$	37·500	1·834	$3{\cdot}832 \times 10^{-4}$	41·658	2·116	3
6	0·07	$4{\cdot}308 \times 10^{-4}$	11·352	0·500	$2{\cdot}715 \times 10^{-4}$	5·347	0·120	$2{\cdot}348 \times 10^{-4}$	7·998	0·817	3
ww	0·15	$5{\cdot}461 \times 10^{-4}$	29·928	3·136	$3{\cdot}769 \times 10^{-4}$	18·840	0·907	$2{\cdot}022 \times 10^{-4}$	12·594	2·040	3
	0·20	$5{\cdot}756 \times 10^{-4}$	45·390	3·492	$4{\cdot}754 \times 10^{-4}$	33·168	2·008	$2{\cdot}401 \times 10^{-4}$	22·338	4·782	3
10	0·07	$5{\cdot}883 \times 10^{-4}$	26·286	1·216	$5{\cdot}497 \times 10^{-4}$	17·154	1·637	$2{\cdot}562 \times 10^{-4}$	20·652	4·530	3
ww	0·15	$7{\cdot}368 \times 10^{-4}$	66·900	11·088	$6{\cdot}462 \times 10^{-4}$	61·920	8·478	$3{\cdot}429 \times 10^{-4}$	38·514	10·914	3
	0·20	$7{\cdot}926 \times 10^{-4}$	104·460	8·448	$7{\cdot}446 \times 10^{-4}$	121·980	5·980	$3{\cdot}468 \times 10^{-4}$	49·884	2·654	3
14	0·07	$4{\cdot}788 \times 10^{-4}$	21·396	1·676	$4{\cdot}087 \times 10^{-4}$	14·982	3·842	$2{\cdot}380 \times 10^{-4}$	11·490	0·493	3
ww	0·15	$5{\cdot}238 \times 10^{-4}$	54·408	15·252	$5{\cdot}169 \times 10^{-4}$	45·996	6·072	$2{\cdot}760 \times 10^{-4}$	36·288	5·741	3
	0·20	$6{\cdot}048 \times 10^{-4}$	81·060	22·170	$5{\cdot}867 \times 10^{-4}$	92·220	6·366	$3{\cdot}288 \times 10^{-4}$	55·746	3·425	3
0	0·07	$6{\cdot}696 \times 10^{-4}$	34·776	2·868	$6{\cdot}090 \times 10^{-4}$	34·902	4·566	$5{\cdot}325 \times 10^{-4}$	30·894	1·282	3
lw	0·15	$6{\cdot}672 \times 10^{-4}$	39·594	2·436	$4{\cdot}929 \times 10^{-4}$	49·482	2·119	$4{\cdot}642 \times 10^{-4}$	30·474	3·891	3
	0·20	$8{\cdot}286 \times 10^{-4}$	63·180	3·064	$5{\cdot}954 \times 10^{-4}$	59·946	5·756	$6{\cdot}552 \times 10^{-4}$	55·914	7·230	3
6	0·07	$5{\cdot}516 \times 10^{-4}$	14·382	0·904	$2{\cdot}963 \times 10^{-4}$	9·810	0·515	$4{\cdot}073 \times 10^{-4}$	14·424	0·562	3
lw	0·15	$4{\cdot}384 \times 10^{-4}$	17·010	0·789	$2{\cdot}218 \times 10^{-4}$	10·356	0·588	$2{\cdot}212 \times 10^{-4}$	8·220	0·280	3
	0·20	$3{\cdot}955 \times 10^{-4}$	19·698	0·970	$1{\cdot}801 \times 10^{-4}$	8·256	0·512	$1{\cdot}448 \times 10^{-4}$	5·587	0·408	3
10	0·07	$3{\cdot}899 \times 10^{-4}$	14·754	0·332	$1{\cdot}899 \times 10^{-4}$	6·990	0·385	$1{\cdot}943 \times 10^{-4}$	11·682	0·682	3
lw	0·15	$1{\cdot}645 \times 10^{-4}$	8·304	1·295	$1{\cdot}003 \times 10^{-4}$	3·229	0·205	$8{\cdot}112 \times 10^{-5}$	4·519	0·647	3
	0·20	$1{\cdot}363 \times 10^{-4}$	5·698	0·358	$6{\cdot}924 \times 10^{-5}$	1·892	0·127	$4{\cdot}554 \times 10^{-5}$	1·846	0·277	3
14	0·07	$1{\cdot}756 \times 10^{-4}$	9·936	0·706	$1{\cdot}117 \times 10^{-4}$	5·759	0·300	$9{\cdot}648 \times 10^{-5}$	8·160	0·583	3
lw	0·15	$8{\cdot}298 \times 10^{-5}$	6·816	1·003	$5{\cdot}328 \times 10^{-5}$	2·629	0·124	$6{\cdot}270 \times 10^{-5}$	2·998	0·248	3
	0·20	$6{\cdot}708 \times 10^{-5}$	4·976	0·187	$4{\cdot}137 \times 10^{-5}$	1·034	0·051	$4{\cdot}314 \times 10^{-5}$	1·799	0·204	3

* Mean values are given in the table; however, statistical analyses are performed with individual data points.

u, horizontal wind velocity (ww, windward; lw, leeward); S_o, slope gradient or channel bottom slope; q, unit discharge; q_s, sediment transport rate; n, replicate.

On the other hand, there were fewer rain intensities with smaller impact angles on leeward slopes as the slope gradient increased, resulting in lower transport rates. Very significantly, differences in the rates between aspects increased as the wind velocity and slope gradient increased. For example, the sediment transport rate on the windward slope was approximately 16 times greater than that on the leeward slope for the rains driven by a 14 m s^{-1} wind incident on a slope of 11·3° for Nukerke silt loam. For the same simulated rains, the rates were 89 and 31 times greater on the windward slopes than on the leeward slopes for Kemmel1 sandy loam and Kemmel2 loam, respectively (Table II and Figure 2).

Raindrop impact and flow interactions played a significant role in determining the sediment transport rate by raindrop-impacted shallow flow under wind-driven rains, and the fluxes of rain energy (Equation 5) and unit discharge and slope (qS_o) satisfactorily explained the rates ($R^2 \geq 78$) (Figure 3).

The statistical fit of Equation 7, which is based on the interaction between raindrop impact and flow parameters, is shown in Table III. All statistical analyses are made with individual data points, although mean values

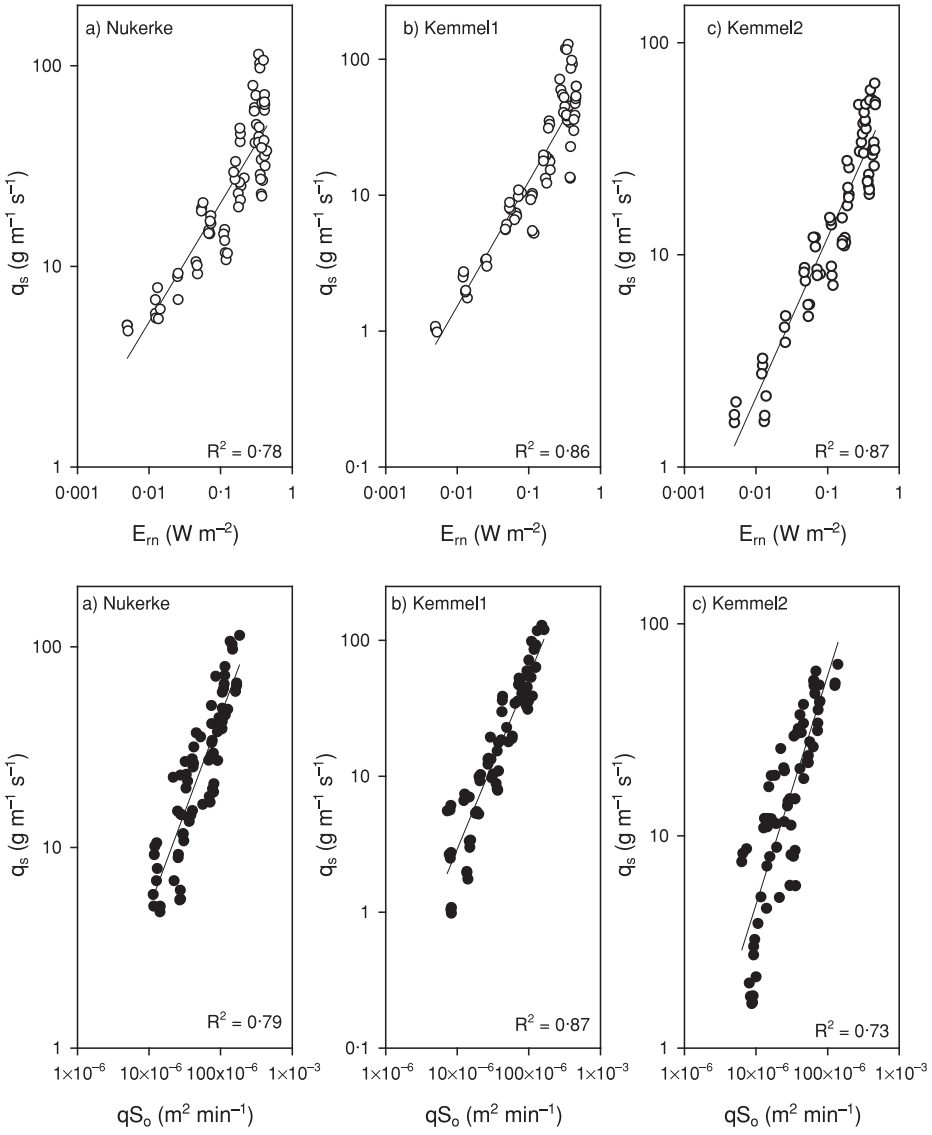

Figure 3. Sediment transport rate by raindrop-impacted shallow flow as a power function of kinetic energy flux and the product of unit discharge and slope for Nukerke silt loam (a), Kemmel1 sandy loam (b), and Kemmel2 loam (c)

Table III. Statistical analyses for the equation* of sediment transport by the raindrop-impacted shallow flow developed by log-linear regression technique for three soils (reprinted from Erpul *et al*., 2003b, with permission from Elsevier)

Soil	k	Prob > |T|	a	Prob > |T|	b	Prob > |T|	c	Prob > |T|	R^2
Nukerke	$3{\cdot}33 \times 10^{-3}$	0·0001	0·45	0·0001	0·34	0·0034	0·65	0·0001	0·91
Kemmel1	$4{\cdot}74 \times 10^{-4}$	0·0001	0·51	0·0002	0·67	0·0009	0·73	0·0001	0·94
Kemmel2	$2{\cdot}27 \times 10^{-3}$	0·0001	0·55	0·0001	0·39	0·0079	0·31	0·0004	0·91

* Equation 7, $q_s = kE_{rn}^a q^b S_o^c$.

are given in Tables I and II, and units of variables are as presented in Tables I and II. The analysis of variance showed that the values of exponents to which the energy flux, unit discharge and slope were raised (a, b and c, respectively) and the soil transport parameter for a shallow flow-driven process k were significant at the level of $\alpha = 0{\cdot}05$ for Nukerke silt loam, Kemmel1 sandy loam and Kemmel2 loam. The models performed reasonably well and accounted for ≥91 per cent of the variations in the shallow flow transport rates.

Additionally, analysis of the Pearson correlation coefficient (r) was carried out to provide the strength of the relation between E_{rn} and q_s and between qS_o and q_s, using the combined data from three soils by:

$$r = \frac{\sum_{i=1}^{N}(E_{rn}q_s) - \frac{\sum_{i=1}^{N}E_{rn}\sum_{i=1}^{N}q_s}{N}}{\sqrt{\left(\sum_{i=1}^{N}E_{rn}^2 - \frac{\left(\sum_{i=1}^{N}E_{rn}\right)^2}{N}\right)\left(\sum_{i=1}^{N}q_s^2 - \frac{\left(\sum_{i=1}^{N}q_s\right)^2}{N}\right)}} \tag{8}$$

Equation (8) exemplifies the r value between E_{rn} and q_s, and $N = 81$ for the analyses performed for windward and leeward rains (3 soils × 3 slope gradients × 3 wind velocities × 3 replicates × 1 aspect). Partitioning of the data of wind-driven rains with respect to the slope aspects indicated that q_s had poorer correlation with E_{rn} and much greater correlation with qS_o in windward slopes (0·55 and 0·88, respectively), which indicated that flow parameters, not the impact parameter, reasonably explained the variation in the sediment transport rate (Table IV), although a larger contribution of raindrop impact was expected due to the greater rain intensities (Table I).

On the other hand, E_{rn} was as much in effect as qS_o for sediment transport in the leeward slopes, and the correlation coefficient between E_{rn} and q_s was 0·91 (Table IV). Evidently, a significant difference occurred not only in the sediment rates but also in flow hydraulics with different aspects under the impact of wind-driven raindrops. This was ascribed to a roughness induced by the directional splashes of soil particles by the inclined raindrop impacts and the contrary lateral stress of impacting raindrops to the direction of the shallow flow.

One would expect by instinct that three types of directional splashes, either submerged or not, appear to exist in our study. First, in the windless rains incident on a slope, particles splashed by raindrop impact flow move downslope or downslope particle movement is more important than the upslope particle movement irrespective of the slope aspect (Figure 4a). In other words, the splash asymmetry of the detached soil particles occurs such that more momentum is transferred in the downslope direction and thus the difference between upslope and downslope transport increases as the slope gradient increases. In this case, lateral raindrop stress is also in the same direction as the shallow flow direction. In fact, raindrop-induced flow resistance empirically estimated by Shen and Li, (1973) and Katz *et al*. (1995) represents this condition of windless rain incident on a slope. Second, in wind-driven rains incident on the windward slopes, the particles splashed by the inclined raindrops are directed upslope, and there is only upslope movement at the threshold, and these particles are captured by the shallow flow running downslope. Clearly, reverse splashes at impact with respect to the shallow flow direction

Table IV. Pearson correlation coefficients (r) among the kinetic energy flux, E_{rn} (W m^{-2})) and the product of flow parameters in the form of qS_o and the sediment transport rate by the raindrop-impacted shallow flow, q_s (g m^{-1} min^{-1}), using combined data from three soils

	E_{rn}	qS_o	q_s
Windless and wind-driven rains			
E_{rn}	1·00 (0·0000)*	0·67 (0·0001)	0·72 (0·0001)
qS_o		1·00 (0·0000)	0·89 (0·0001)
q_s			1·00 (0·0000)
Wind-driven rains			
E_{rn}	1·00 (0·0000)	0·76 (0·0001)	0·86 (0·0001)
qS_o		1·00 (0·0000)	0·92 (0·0001)
q_s			1·00 (0·0000)
Windward rains			
E_{rn}	1·00 (0·0000)	0·45 (0·0001)	0·55 (0·0001)
qS_o		1·00 (0·0000)	0·88 (0·0001)
q_s			1·00 (0·0000)
Leeward rains			
E_{rn}	1·00 (0·0000)	0·75 (0·0001)	0·92 (0·0001)
qS_o		1·00 (0·0000)	0·91 (0·0001)
q_s			1·00 (0·0000)

* Numbers in parentheses are significance levels.

occur, and this, together with contrary lateral raindrop stress that increases as the horizontal wind velocity increases, forms such raindrop-induced roughness that greater flow depth could occur, increasing the dissipation of the raindrop impact energy (Figure 4b). Third, in the wind-driven rains incident on the leeward slopes, the particles splashed by the inclined raindrops are directed downslope and thus, being in the same direction as the shallow flow direction (Figure 4c) and similar to the first case, the lateral raindrop stress is also in the same direction as the shallow flow. The only difference from the first case is the unidirectional downslope particle movement without any upslope component of particle movement in this case.

As shown in Figure 4, different hydraulics of shallow flow might occur depending on wind velocity and direction. Our analysis of Pearson correlation coefficients (Equation 8 and Table IV) appeared to reflect these differences. E_{rn} was poorly correlated with q_s, and qS_o tended to dominate as flow depth increased in the windward slopes while E_{rn} performed equally as well as qS_o, explaining more than 90 per cent of the variation of q_s on the leeward slopes. Reverse splashes of particles and reverse lateral raindrop stress with respect to the shallow flow direction worked together to lead to more deepened flow in the windward slopes giving rise to the decreased contribution of raindrop impact to sediment transport on these slopes.

CONCLUSIONS

Experimental results directly taken on wind effects on sediment transport by raindrop-impacted shallow flow have been presented in this study, aiming to provide a better insight into the process under wind-driven rains. Flux of rain energy computed by combining the effects of wind on the velocity, frequency, and angle of raindrop impact and unit discharge and slope adequately described the characteristics of wind-driven rains and significantly explained the variations in sediment delivery rates to shallow flow transport ($R^2 \geq 0{\cdot}91$). Analyses of the Pearson correlation coefficients additionally showed that a significant difference occurred in shallow flow hydraulics with different aspects under the impacts of wind-driven raindrops. The reverse/advance particle splashes and the lateral stress of impacting raindrops at an angle with respect to the shallow flow direction were concluded to have significant effects on the shallow flow hydraulics under wind-driven rains. However, there is a need for further experimentation to parameterize these roughness elements, and an understanding of these mechanisms should facilitate the development of robust models to assess the sediment transport by raindrop-impacted shallow flow under wind-driven rains.

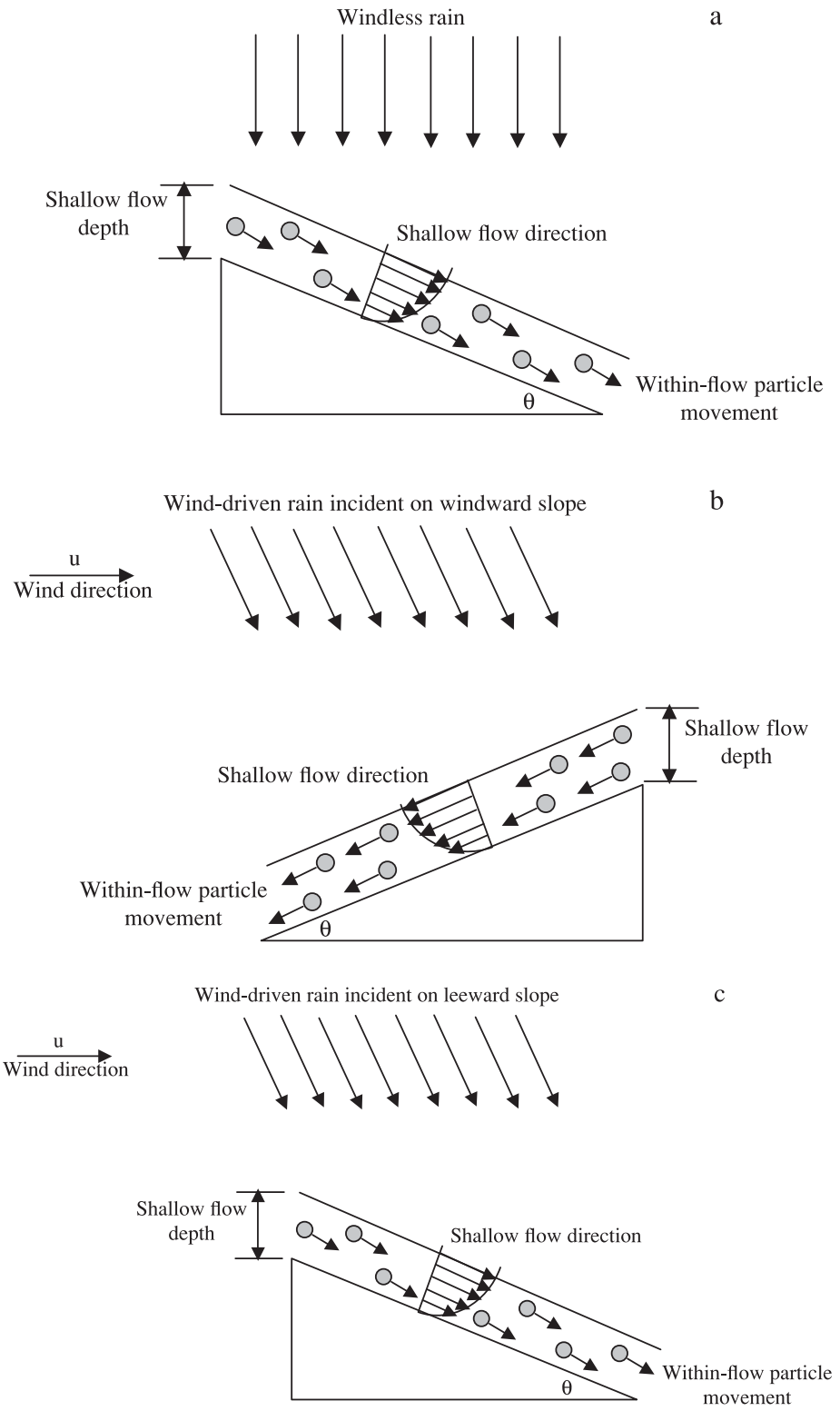

Figure 4. Within-flow particle movements under windless rain on a slope (a), wind-driven rain on a windward slope (b), and wind-driven rain on a leeward slope (c)

REFERENCES

De Lima JLMP. 1989a. Overland flow under simulated wind-driven rain. *Proceedings of the 11th International Congress on Agricultural Engineering*, Dublin, 4–8 September: 493–500.

De Lima JLMP. 1989b. Raindrop splash anisotropy: Slope, wind and overland flow velocity effects. *Soil Technology* **2**: 71–78.

De Lima JLMP. 1989c. The influence of the angle of incidence of the rainfall on the overland flow processes. *New Directions for Surface Water Modelling* (Proceedings of the Baltimore Symposium, May 1989). IAHS Publication No. **181**: 73–82.

De Lima JLMP. 1990. The effect of oblique rain on inclined surfaces: A nomograph for the rain-gauge correction factor. *Journal of Hydrology* **115**: 407–412.

De Lima JLMP, Singh VP, De Lima MIP. 2003. The influence of storm movement on water erosion: storm direction and velocity effects. *Catena* **52**: 39–56.

Disrud, LA. 1970. Magnitude, probability, and kinetic energy of winds associated with rains in Kansas. *Transactions Kansas Academy of Science* **73**(2): 237–246.

Erpul G, Gabriels D, Janssens D. 1998. Assessing the drop size distribution of simulated rainfall in a wind tunnel. *Soil and Tillage Research* **45**: 455–463.

Erpul G, Gabriels D, Janssens D. 2000. The effect of wind on size and energy of small simulated raindrops: a wind tunnel study. *International Agrophysics* **14**: 1–7.

Erpul G, Norton LD, Gabriels D. 2002. Raindrop-induced and wind-driven soil particle transport. *Catena* **47**: 227–243.

Erpul G, Norton LD, Gabriels D. 2003a. The effect of wind on raindrop impact and rainsplash detachment. *Transactions of the ASAE* **45**(6): 51–62.

Erpul G, Norton LD, Gabriels D. 2003b. Sediment transport from interill areas under wind-driven rain. *Journal of Hydrology* **276**: 184–197.

Foster, GR. 1982. Modeling the soil erosion process. In *Hydrologic Modeling of Small Watersheds*, Haan CT, Johnson HP, Brakensiek DL (eds). ASAE Monograph No. 5. ASAE: St. Joseph, MI; 297–382.

Gabriels D, Cornelis W, Pollet I, Van Coillie T, Quessar M. 1997. The I.C.E. wind tunnel for wind and water erosion studies. *Soil Technology* **10**: 1–8.

Gerits J, De Lima JLMP. 1990. Solute transport and wind action in relation to overland flow and water erosion. *Catena Supplement* **17**: 67–78.

Ghadiri H, Payne D. 1980. A study of soil splash using cine-photography. In *Assessment of Erosion*, De Boodt M, Gabriels D (eds). John Wiley and Sons: Chichester; 185–192.

Ghadiri H, Payne D. 1981. Raindrop impact stress. *Journal of Soil Science* **32**: 41–49.

Gilley JE, Finkner SC. 1985. Estimating soil detachment caused by raindrop impact. *Transactions of the ASAE* **28**(1): 140–146.

Gilley JE, Woolhiser DA, McWhorter DB. 1985. Interrill soil erosion. Part I: Development of model equations. *Transactions of the ASAE* **28**(1): 147–153, 159.

Guy BT, Dickinson WT, Rudra RP. 1987. The roles of rainfall and runoff in the sediment transport capacity of interrill flow. *Transactions of the ASAE* **30**(5): 1378–1386.

Helming K. 2001. Wind speed effects on rain erosivity. In *Sustaining the Global Farm*, In Soil Conservation Organization Meeting, 24–29 May 1999, Stott DE, Mohtar RH, Steinhardt GC. (eds). USDA-ARS National Soil Erosion Research Laboratory: West Lafayette, Indiana; 771–776.

Heymann FJ. 1967. A survey of clues to the relation between erosion rate and impact parameters. *Second Rain Erosion Conference* **2**: 683–760.

Julien PY, Simons DB. 1985. Sediment transport capacity of overland flow. *Transactions of the ASAE* **28**: 755–762.

Katz DM, Watts FJ, Burroughs ED. 1995. Effects of surface roughness and rainfall impact on overland flow. *Journal of Hydraulic Engineering* **121**(7): 546–553.

Kinnell PIA. 1988. The influence of flow discharge on sediment concentrations in raindrop induced flow transport. *Australian Journal of Soil Research* **26**: 575–582.

Kinnell PIA. 1990. The mechanics of raindrop-induced flow transport. *Australian Journal of Soil Research* **28**(4): 497–516.

Kinnell PIA. 1993. Interrill erodibilities based on the rainfall intensity-flow discharge erosivity factor. *Australian Journal of Soil Research* **31**: 319–332.

Moss AJ, Green P. 1983. Movement of solids in air and water by raindrop impact. Effects of drop-size and water-depth variations. *Australian Journal of Soil Research* **21**(3): 373–382.

Mutchler CK. 1967. Parameters for describing raindrop splash. *Journal of Soil and Water Conservation*, **22**(3): 91–94.

Mutchler CK, Larson CL. 1971. Splash amounts from waterdrop impact on a smooth surface. *Water Resources Research* **7**: 195–200.

Mutchler CK, Young RA. 1975. Soil detachment by raindrops. In *Present and prospective technology for predicting sediment yields and sources*. ARS, 1-S-40. USDA: 113–117.

Parsons AJ, Stromberg SGL, Greener M. 1998. Sediment-transport competence of rain-impacted interrill overland flow. *Earth Surface Processes and Landforms* **23**: 365–375.

Pedersen HS, Hasholt B. 1995. Influence of wind speed on rainsplash erosion. *Catena* **24**: 39–54.

Poesen J, Savat J. 1981. Detachment and transportation of loose sediments by raindrop splash. Part II: Detachability and transportability measurements. *Catena* **8**: 19–41.

SAS, 1995. *SAS System for Elementary Statistical Analysis*. SAS Inst. Inc.: Cary, NC; 280–285.

Sellers WD. 1965. *Physical Climatology*. University of Chicago Press: Chicago.

Sharon D. 1980. The distribution of hydrologically effective rainfall incident on sloping ground. *Journal of Hydrology* **46**: 165–188.

Shen HW, Li RW. 1973. Rainfall effect on sheet flow over smooth surfaces. *Journal of the Hydrology Division American Society of Civil Engineers* May: 771–792.

Springer GS. 1976. *Erosion by Liquid Impact*. John Wiley and Sons: New York.

Torri D, Sfalanga M, Del Sette M. 1987. Splash detachment: runoff depth and soil cohesion. *Catena* **14**: 149–155.

Zhang XC, Nearing MA, Miller WP, Norton LD, West LT. 1998. Modeling interrill sediment delivery. *Soil Science Society of America Journal* **62**: 438–444.

